

Brief communication

Dipole model of vorticity at the moving contact line

Peter Zhang^a, Kamran Mohseni^{a,b,*}^a Department of Mechanical and Aerospace, University of Florida, Gainesville, FL, United States^b Department of Electrical and Computer Engineering, University of Florida, Gainesville, FL, United States

ARTICLE INFO

Article history:

Received 14 September 2017

Revised 9 January 2018

Accepted 10 February 2018

Available online 17 February 2018

Keywords:

Vorticity dipole

Multiphase

Moving contact line

1. Introduction

Vorticity, defined as the curl of velocity ($\omega \equiv \nabla \times \mathbf{u}$), has become a topic of significant interest over the past century. As a measure of local fluid rotation, vorticity has proven to be useful for characterizing a variety of natural phenomena. While vorticity is not a primary variable such as velocity or pressure, it contains a wealth of information that is invaluable to a variety of fields including aerodynamics (Brown and Michael, 1954; Graham, 1983; Katz, 1981; Karman and Sears, 1938; Sedov et al., 1965; Wu, 1981), turbulence (Chorin, 1996; McWilliams, 1984; Grant, 1958; Hussain, 1986), and mixing (Sutera, 1965; Jacobi and Shah, 1995; Mehdizadeh et al., 2011; Zhang and Mohseni, 2014). The importance of vorticity has been well recognized and we refer the reader to the works of Truesdell (1954), Lim and Nickels (1995), Saffman (1992), and Wu et al. (2006) for a general discussion of the generation, dynamics, and decay of vorticity. Among these publications, the discussion of vorticity generation is often focused on smooth solid interfaces. However, as the complexity of physical problems continues to grow, there is a clear need to develop a better understanding of vorticity and vorticity generation in complex geometries and multiphase flows.

In this manuscript, we are motivated by the work of DeVoria and Mohseni (2015) to examine the vorticity near corner singularities along a fluid interface, or the moving contact line (MCL). In their investigation, the authors performed a detailed study of translating droplets using micro-particle image ve-

locimetry (micro-PIV). They observed high concentrations of vorticity near the MCL in addition to a vorticity sign change near the droplet interface, see Fig. 1. In the lower left quadrant of the droplet, flow near the trailing contact line is captured and shows strong concentrations of negative vorticity as expected. However, small patches of positive vorticity appear along the trailing interface, leading one to question the source of this opposite signed vorticity. The authors attributed this vorticity to boundary layers on the fluid-gas interface, but suspected that vorticity was being generated at the moving contact line. However, vorticity at the MCL was outside the scope of their investigation and thus they did not pursue this topic.

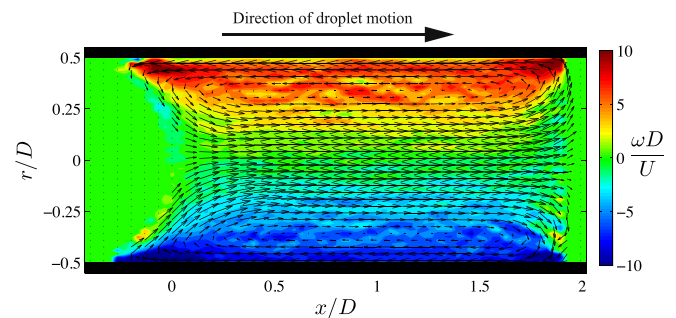


Fig. 1. Velocity and vorticity field of a water droplet translating in a microchannel. Velocity is plotted relative to a reference frame moving with the droplet. Data was collected using particle image velocimetry. Significant vorticity is apparent near both the leading and trailing triple contact points; indicating the possibility of a vorticity source at these locations. The droplet has a length to height ratio of 2 and a Reynolds number of approximately 6.5. Reproduced from DeVoria and Mohseni (2015).

* Corresponding author at: Department of Mechanical and Aerospace, University of Florida, Gainesville, FL, United States.

E-mail address: mohseni@ufl.edu (K. Mohseni).

In this paper, we build on the work of DeVoria & Mohseni by performing a theoretical investigation and experimental validation of vorticity at the moving contact line. Section 2 introduces an analytic model for vorticity at the MCL and demonstrates that the vorticity has a dipole distribution. This vorticity dipole indicates that the MCL is a dipole source of vorticity that allows opposite sign vorticity generation. Section 3 compares the vorticity dipole solution with experimental data and continuum numerical simulations. Conclusions of this investigation are given in Section 4.

2. Dipole model of vorticity at the MCL

In a small region adjacent to the moving contact line, the interface geometry can be approximated by a corner, as seen in Fig. 2(a). r and θ define a local polar coordinate system centered at the moving contact line, ϕ denotes the apparent dynamic contact angle, and the boundaries of the corner represent the fluid-solid and fluid-gas interface. At the boundaries, the fluid has a velocity \mathbf{u}_a and \mathbf{u}_b . If this region is small, such that the local Reynolds number is significantly smaller than 1 ($Re = \rho U r / \mu \ll 1$), then the flow is governed by the Stokes equation which is given by

$$\nabla p = \mu \nabla^2 \mathbf{u}, \quad (1)$$

where p denotes the pressure, ρ the density, U the mean velocity, μ the dynamic viscosity, and \mathbf{u} the fluid velocity. The governing equation for vorticity in a Stokes flow is given by

$$\nabla^2 \omega = 0, \quad (2)$$

and can be obtained by taking the curl of Eq. (1). As a first order approximation, we set \mathbf{u}_a and \mathbf{u}_b to be constants and find that the solution for vorticity near a moving contact line is given by

$$\omega = \frac{\alpha}{r} \cos(\theta - \beta). \quad (3)$$

Details of the solution method and exact analytical relations for the coefficients α and β can be found in Appendix A.

Fig. 2(b) shows an example of the vorticity distribution near a moving contact line with an apparent contact angle of 60° and interface velocities given by $u_r(\theta = 0) = 1$, $u_r(\theta = \phi) = -1$ and $u_\theta(\theta = 0, \phi) = 0$. While the flow only occupies the domain $0^\circ \leq \theta \leq 60^\circ$, we have plotted vorticity field for $0^\circ \leq \theta \leq 360^\circ$ to illustrate that the vorticity solution forms a dipole. Therefore, the coefficients α and β represent the strength and orientation of the

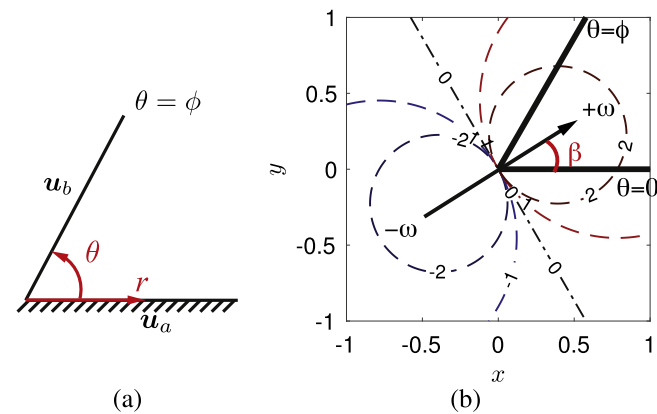


Fig. 2. (a) Schematic of the moving contact line. A polar coordinate system (r, θ) is defined with its origin centered at the corner point. \mathbf{u}_a and \mathbf{u}_b are the fluid velocities along the fluid-solid and fluid-gas interfaces respectively. (b) Theoretical model for vorticity near a moving contact line as described in Section 2. The interfaces are denoted by the solid black lines and form an apparent contact angle of $\phi = 60^\circ$. Fluid velocity at the interfaces is given by $u_r(\theta = 0) = 1$, $u_r(\theta = \phi) = -1$, and $u_\theta(\theta = 0, \phi) = 0$. The arrow denotes the dipole moment vector with magnitude α and orientation β .

dipole. According to this model, any moving contact line flow with constant interface velocities will contain a simple vorticity dipole. Furthermore, this result predicts a non-zero radial vorticity gradient as $r \rightarrow 0$, indicating that vorticity is generated at the moving contact line. Because this vorticity generation can be positive and negative, a portion of the opposite signed vorticity observed in DeVoria and Mohseni (2015) originates from the contact line. The amount of positive and negative vorticity is determined by α and β , which are functions of the interface velocity and apparent contact angle only. As such, the vorticity dipole strength and orientation are determined easily from macroscopically observed quantities. In practice, one could use this knowledge to treat a surface and control contact angle such that vorticity generation is either increased or decreased depending on the application. In dynamic applications, the contact angle could even be manipulated on demand using techniques such as electrowetting (Mugele and Baret, 2005; Baird et al., 2007). Despite this relatively simple model, the following sections will demonstrate that the vorticity dipole is consistent with experimental data and numerical simulations.

3. Comparison with numerical and experimental results

In order to validate the vorticity dipole model, we will compare the theoretical model with the micro-PIV data originally presented by DeVoria and Mohseni (2015) in addition to a matching numerical simulation. Specifically, we will examine the lower left receding contact line of the droplet shown in Fig. 1. The parameters of this example are extracted from the experiment, which yields a droplet aspect ratio of two and $Re_D = \rho U D / \mu = 6.5$ where D denotes the diameter of the channel. Details regarding the experimental setup can be found in DeVoria and Mohseni (2015). The numerical simulation is conducted using Gerris (Popinet, 2003), where the multiphase flow was simulated using the volume of fluid (VOF) method and surface tension effects were captured using the continuum-surface-force method (Popinet, 2009). The numerical simulation was run using a leading edge contact angle of 90° , a trailing edge contact angle of 30° , and a droplet Reynolds number matching the experiment. Grid size was set to $D/256$.

In Fig. 3(a) and (b), the theoretical velocity and vorticity field of the 30° receding contact line is shown. At the interfaces, the velocity is set to $u_r(\theta = 0) = -U$ and $u_r(\theta = \phi) = 0.4U$ based on the interface velocities experimentally measured by DeVoria & Mohseni, where U is the mean velocity of the droplet. Given these boundary conditions, the theoretical solution predicts a dipole strength of $\alpha = 13.4$ and a dipole orientation of $\beta = 116^\circ$. As expected, the theoretical velocity field circulates in a clockwise direction and corresponds to a vorticity field that is primarily negative. However, near the fluid-gas interface, there exists a small region of positive vorticity, as predicted by β , the vorticity dipole orientation. Thus the theoretical model predicts a dipole source of vorticity that generates both positive and negative vorticity. In the discussion below, we find that the experimental droplet, Fig. 3(c and d), and the numerical simulation, Fig. 3(e and f), are in excellent agreement with our theoretical model.

The experimental droplet exhibits vorticity that is primarily negative in the bottom half and primarily positive in the upper half. Near the lower left receding contact line, magnified in Fig. 3(d), there are high concentrations of negative vorticity and a small region of positive vorticity near the fluid-gas interface, in agreement with our theoretical predictions. If we superimpose the theoretical zero vorticity contour, denoted by the dash-dotted line, we observe excellent agreement in β , the vorticity dipole orientation. At present, we are unable to experimentally compare the dipole strength, as data near the MCL is not available due to limitations of the experimental setup.

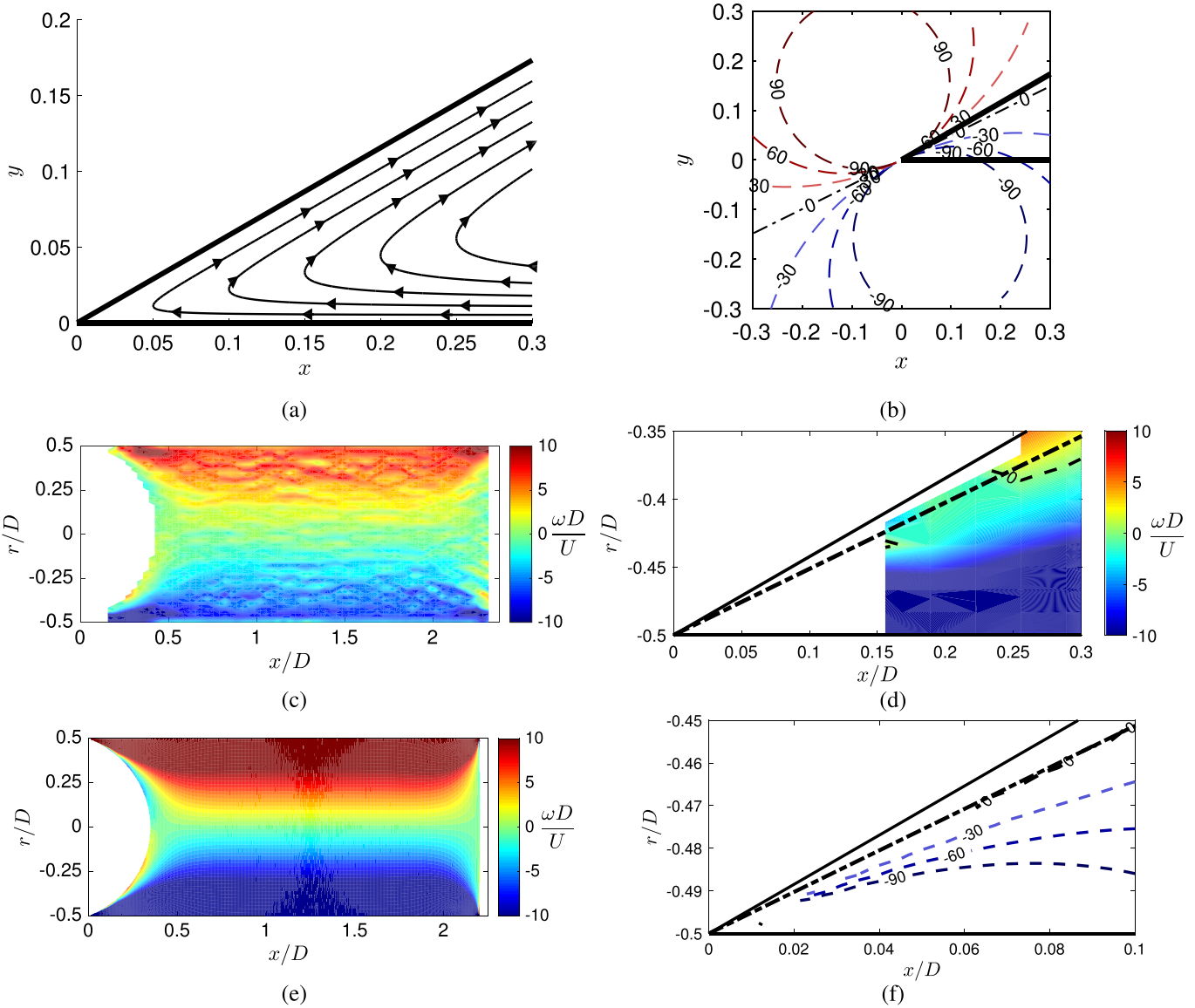


Fig. 3. (a) Velocity field of a 30° viscous corner flow analytically determined using Eq. (1). Boundary conditions are $u_\theta(\theta = 0) = u_\theta(\theta = \phi) = 0$, $u_r(\theta = 0) = -U$, and $u_r(\theta = \phi) = 0.4U$ where U denotes the velocity of the droplet. (b) Vorticity contours analytically determined using Eq. (3) for $0^\circ \leq \theta < 360^\circ$ where solid lines (—) denote the boundaries of the corner, the dashed line (---) denote vorticity contours of constant magnitude, and the dash-dotted line (-.-.-) denotes the vorticity contour of magnitude 0. (c) Experimentally measured vorticity field of a droplet translating in a microchannel. Reproduced from DeVoria and Mohseni (2015). (d) Experimentally measured vorticity field near the trailing edge of the droplet pictured in Fig. 1 (DeVoria and Mohseni, 2015). The dash-dotted line (-.-.-) denotes the analytically computed zero vorticity contour while the dashed line (---) denotes the experimentally measured zero vorticity contour. (e) Numerical simulation of the Navier–Stokes equation for a droplet translating in a microchannel with a trailing edge contact angle of 30°, leading edge contact angle of 90°, $Re_D = 6.5$, $Ca = 0.003$, and a grid size of $D/256$. (f) Trailing edge of the numerically simulated droplet translating in a microchannel. The dash-dotted line (-.-.-) denotes the analytically computed zero vorticity contour while the dashed lines (---) denote the numerically predicted vorticity contours.

The numerically simulated droplet, shown in Fig. 3(e), matches the experimental droplet in both shape and vorticity distribution. At the lower left receding contact line, we once again observe high concentrations of negative vorticity, with a small region of positive vorticity. With the resolution of the numerical simulation, it is clear that the positive vorticity extends to the MCL and is created by the vorticity dipole source. Once again, we can superimpose the theoretical zero vorticity contour, and show that the theoretical, experimental, and numerical dipole orientation are all in agreement with each other. From the numerical vorticity field, we can also extract the dipole strength, which yields $\alpha_{num} = 13.9$, and is in agreement with the theoretically predicted dipole strength of $\alpha = 13.4$. From these comparisons, we conclude that the vorticity dipole is an accurate model of vorticity near the MCL.

4. Conclusion

In this manuscript vorticity near a moving contact line was investigated theoretically. By assuming a relatively simple corner geometry and constant interface velocities, we found that vorticity near the MCL is modeled by a vorticity dipole. The strength and orientation of this dipole was identified analytically and found to be a function of the apparent contact angle and interface velocity only. Given this dipole distribution, the theoretical model indicates that both positive and negative vorticity can be generated at the moving contact line. When compared with experimental micro-PIV data and numerical simulations, the vorticity dipole shows excellent agreement despite the simplicity of the model. A detailed examination of the MCL shows that the theoretical dipole model is

even capable of capturing the small regions of opposite signed vorticity observed on the droplet interface. In the future, this model of vorticity could be used to manipulate mixing in multiphase flows via contact angle modification.

Acknowledgements

We wish to acknowledge the Office of Naval Research grant no. N00014-17-1-2346 for their support in this research effort. We would also like to thank Dr. Adam DeVoria for and Joseph Thakkottor for their helpful discussion.

Appendix A. Theoretical solution of vorticity near a MCL

The Stokes flow in a semi-infinite corner is governed by the Stokes equation given by

$$\nabla p = \mu \nabla^2 \mathbf{u}.$$

By taking the curl of the Stokes equation and applying the relation $\omega = -\nabla^2 \psi$, we obtain

$$\nabla^4 \psi = 0, \quad \nabla^2 \omega = 0,$$

where ψ denotes the stream function. Using the method of separation of variables one finds that the general stream function solution is given by

$$\psi = P_n r^n f_n(\theta) + Q_0 \ln r g_0(\theta) + Q_1 r \ln r g_1(\theta) + Q_2 r^2 \ln r g_2(\theta),$$

where P and Q are dimensional constants. This solution is consistent with the those found in [Michell \(1899\)](#) and [Filonenko-Borodich \(1958\)](#). The stream function solution for the flow near a moving contact line is determined by applying the boundary conditions $u_\theta(\theta = 0) = u_\theta(\theta = \phi) = 0$, $u_r(\theta = 0) = U_a$, and $u_r(\theta = \phi) = u_b(r)$. To simplify the analysis, we expand $u_b(r)$ using a Taylor series, that is

$$u_b(r) = \sum_{k=0}^{\infty} \frac{u_b^{(k)}(r=0)r^k}{k!} = U_b + u_b'(r=0)r + \dots$$

Solving the biharmonic stream function equation yields a stream function and vorticity field given by

$$\psi = U_a r f_{1,a} + U_b r f_{1,b} + \sum_{n=2}^{\infty} \frac{u_b^{(n-1)} r^n f_{n,b}}{4(n-1)!},$$

$$\omega = \frac{U_a}{r} [f_{1,a} + f_{1,a}'] + \frac{U_b}{r} [f_{1,b} + f_{1,b}'] + \sum_{n=2}^{\infty} \frac{u_b^{(n-1)} r^{n-2}}{4(n-1)!} [n(n-1)f_{n,b} + n f_{n,b} + f_{n,b}'],$$

where f_n is given by

$$\begin{aligned} f_1 &= A_1 \cos(\theta) + B_1 \sin(\theta) + C_1 \theta \cos(\theta) + D_1 \theta \sin(\theta), \\ f_2 &= A_2 + B_2 \theta + C_2 \cos(2\theta) + D_2 \sin(2\theta), \\ f_n &= A_n \cos((n-2)\theta) + B_n \cos(n\theta) + C_n \sin((n-2)\theta) \\ &\quad + D_n \sin(n\theta). \end{aligned}$$

A , B , C , and D are coefficients determined by the boundary conditions. As before, we assume that r is small so that the local Reynolds number is small, and find that the vorticity field is dominated by the term that scales with r^{-1} , otherwise known as the vorticity dipole. Because the vorticity dipole is solely generated by U_a and U_b , we can simplify the problem by taking a first order approximation and estimating the interface velocities as constants. The stream function and vorticity distribution corresponding to constant interface velocities are given by

$$\psi = U_a r f_{1,a}(\theta) + U_b r f_{1,b}(\theta),$$

$$\omega = \frac{U_a}{r} [f_{1,a}(\theta) + f_{1,a}'(\theta)] + \frac{U_b}{r} [f_{1,b}(\theta) + f_{1,b}'(\theta)]$$

$$= \frac{\alpha}{r} \cos(\theta - \beta),$$

where α and β are given by

$$\begin{aligned} \alpha &= 2 \left[\left(\frac{\sin(\phi)^4 + (\phi - \cos(\phi) \sin(\phi))^2}{(\sin(\phi)^2 - \phi^2)^2} \right) U_a^2 \right. \\ &\quad + \left(\frac{2\phi \sin(\phi)^3 + 2(\phi - \cos(\phi) \sin(\phi))(\sin(\phi) - \phi \cos(\phi))}{(\sin(\phi)^2 - \phi^2)^2} \right) U_a U_b \\ &\quad \left. + \left(\frac{(\sin(\phi) - \phi \cos(\phi))^2 + \phi^2 \sin(\phi)^2}{(\sin(\phi)^2 - \phi^2)^2} \right) U_b^2 \right]^{1/2}, \\ \beta &= -\tan^{-1} \left(\frac{(-2 \sin(\phi)^2) U_a + (-2\phi \sin(\phi)) U_b}{(\sin(2\phi) - 2\phi) U_a + (2\phi \cos(\phi) - 2 \sin(\phi)) U_b} \right) + \pi. \end{aligned}$$

While this investigation only considers the vorticity corresponding to $n = 1$, other Stokes flows corresponding to various values of n have been investigated in [Moffatt \(1964\)](#), [Huh and Scriven \(1971\)](#), [Gelderblom et al. \(2012\)](#) and [Richardson \(1968\)](#).

References

- Baird, E., Young, P., Mohseni, K., 2007. Electrostatic force calculation for an EWOD-actuated droplet. *Microfluid. Nanofluidics* 3 (6), 635–644. doi:10.1007/s10404-006-0147-y.
- Brown, C.E., Michael, W.H., 1954. Effect of leading-edge separation on the lift of a delta wing. *J. Aeronaut. Sci.* 21 (10), 690–694.
- Chorin, A.J., 1996. *Vorticity and Turbulence*. Springer-Verlag, New York City, NY, USA.
- DeVoria, A.C., Mohseni, K., 2015. Droplets in an axisymmetric microtube: effects of aspect ratio and fluid interfaces. *Phys. Fluids* 27 (1), 012002(1–18). doi:10.1063/1.4904753.
- Filonenko-Borodich, M., 1958. *Theory of Elasticity*. University Press of the Pacific, Moscow.
- Gelderblom, H., Bloemen, O., Snoeijer, J., 2012. Stokes flow near the contact line of an evaporating drop. *J. Fluid Mech.* 709, 69–84.
- Graham, J.M.R., 1983. The lift on an aerofoil in starting flow. *J. Fluid Mech.* 133, 413–425.
- Grant, H., 1958. The large eddies of turbulent motion. *J. Fluid Mech.* 4 (02), 149–190.
- Huh, C., Scriven, L.E., 1971. Hydrodynamic model of steady movement of a solid/liquid/fluid contact line. *J. Colloid Interface Sci.* 35 (1), 85–101. doi:10.1016/0021-9797(71)90188-3.
- Hussain, A., 1986. Coherent structures and turbulence. *J. Fluid Mech.* 173, 303–356.
- Jacobi, A., Shah, R., 1995. Heat transfer surface enhancement through the use of longitudinal vortices: a review of recent progress. *Exp. Therm. Fluid Sci.* 11 (3), 295–309.
- Karman, T.V., Sears, W.R., 1938. Airfoil theory for non-uniform motion. *J. Aeronaut. Sci.* 5 (10), 379–390.
- Katz, J., 1981. A discrete vortex method for the non-steady separated flow over an airfoil. *J. Fluid Mech.* 102, 315–328. doi:10.1017/S0022112081002668.
- Lim, T.T., Nickels, T.B., 1995. Vortex rings. In: Green, S.I. (Ed.), *Fluid Vortices*. Springer-Verlag, New York City, NY, USA, pp. 95–153.
- McWilliams, J.C., 1984. The emergence of isolated coherent vortices in turbulent flow. *J. Fluid Mech.* 146, 21–43. doi:10.1017/S0022112084001750.
- Mehdizadeh, A., Sherif, S.A., Lear, W.E., 2011. Numerical simulation of thermofluid characteristics of two-phase slug flow in microchannels. *Int. J. Heat Mass Transf.* 54 (15–16), 3457–3465. doi:10.1016/j.ijheatmasstransfer.2011.03.040.
- Michell, J., 1899. On the direct determination of stress in an elastic solid, with application to the theory of plates. *Proc. London Math. Soc.* 1 (1), 100–124.
- Moffatt, H.K., 1964. Viscous and resistive eddies near a sharp corner. *J. Fluid Mech.* 18 (01), 1–18.
- Mugele, F., Baret, J.C., 2005. Electrowetting: from basics to applications. *J. Phys.* 17 (28), 705–774. doi:10.1088/0953-8984/17/28/R01.
- Popinet, S., 2003. Gerris: a tree-based adaptive solver for the incompressible euler equations in complex geometries. *J. Comput. Phys.* 190 (2), 572–600. doi:10.1016/S0021-9991(03)00298-5.
- Popinet, S., 2009. An accurate adaptive solver for surface-tension-driven interfacial flows. *J. Comput. Phys.* 228 (16), 5838–5866. doi:10.1016/j.jcp.2009.04.042.
- Richardson, S., 1968. Two-dimensional bubbles in slow viscous flows. *J. Fluid Mech.* 33 (03), 475–493.
- Saffman, P.G., 1992. *Vortex Dynamics*. Cambridge University Press, Cambridge, UK.
- Sedov, L.I., Chu, C.K., Cohen, H., Seckler, B., Gillis, J., 1965. Two-dimensional problems in hydrodynamics and aerodynamics. *Phys. Today* 18 (12), 62–63. doi:10.1063/1.3047038.
- Sutera, S., 1965. Vorticity amplification in stagnation-point flow and its effect on heat transfer. *J. Fluid Mech.* 21 (03), 513–534.
- Truesdell, C., 1954. *The Kinematics of Vorticity*. Indiana University Press, Bloomington, IA, USA.
- Wu, J.C., 1981. Theory for aerodynamic force and moment in viscous flows. *AIAA J.* 19 (4), 432–441.
- Wu, J.-Z., Ma, H.-Y., Zhou, M.-D., 2006. *Vorticity and Vortex Dynamics*. Springer.
- Zhang, P., Mohseni, K., 2014. A unified model for digitized heat transfer in a microchannel. *Int. J. Heat Mass Transf.* 78, 393–407. doi:10.1016/j.ijheatmasstransfer.2014.06.018.